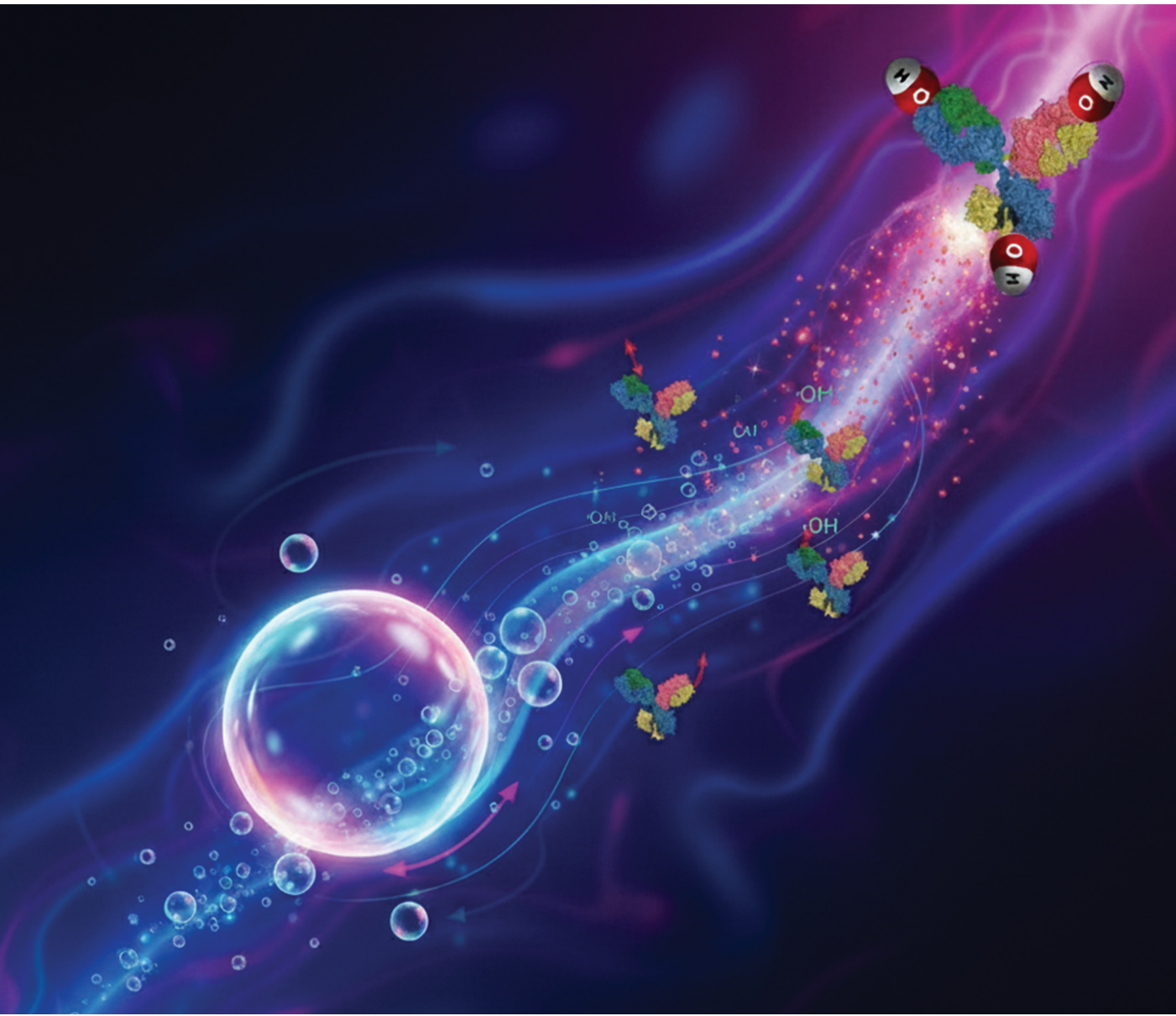


# Materials Advances

[rsc.li/materials-advances](http://rsc.li/materials-advances)



ISSN 2633-5409

## COMMUNICATION

Ha M. Nguyen *et al.*

Enhanced treatment uniformity of chemical and biological liquids in cold atmospheric plasma system using gas bubble mixing



Cite this: *Mater. Adv.*, 2025, 6, 9364

Received 27th August 2025,  
Accepted 16th November 2025

DOI: 10.1039/d5ma00963d

rsc.li/materials-advances

## Enhanced treatment uniformity of chemical and biological liquids in cold atmospheric plasma system using gas bubble mixing

Ha M. Nguyen, <sup>a,b</sup> Haoyu Cheng, <sup>a</sup> Yuting Wu, <sup>a,c</sup> Benjamin B Minkoff, <sup>d</sup> Thao T. Nguyen, <sup>dg</sup> Mark P. Richards, <sup>c</sup> Michael R. Sussman, <sup>d</sup> Hau D. Le <sup>bef</sup> and J. Leon Shohet<sup>a</sup>

**Achieving uniform liquid treatment with cold atmospheric plasma (CAP) is vital for aqueous chemical and biological samples, especially for oxidation- and heat-sensitive substances such as proteins. However, attaining this goal remains a key challenge in the realm of plasma–liquid interactions. The difficulty arises from the limited liquid penetration of short-lived reactive species generated on the liquid surface, the heat produced when plasma forms in bulk liquid, and the instability of plasma bubbles generated in the liquid. Here, we report a gas bubble mixing approach to improve the uniformity of liquid treatment (ULT). The key idea is that the laminar wake created by a single bubble rising in a liquid serves as an efficient mixing mechanism that enhances ULT without compromising CAP stability. By integrating gas bubble mixing into a PLIMB (Plasma-induced Modification of Biomolecules)-based CAP–liquid reactor, we demonstrate a notable improvement in both ULT and treatment time for various liquid samples containing organic molecules. This strategy may be broadly extended to cold atmospheric plasma treatments of diverse functional material systems—such as drug-delivery exosomes, micelles, and plasma-aided surface-engineered nanoparticles—suspended or dissolved in liquids, enabling advances in plasma-aided processing of chemical and biological materials in their aqueous environments.**

### 1. Introduction

Cold atmospheric plasma (CAP) is a partially ionized gas with potential applications as a source of reactive oxygen and

nitrogen species (RONS), such as hydroxyl radicals (OH radicals), in synergy with others such as photons, electrons, ions, magnetic and electric fields, and minimal heat.<sup>1–6</sup> CAP can be generated conveniently at or near room temperature and atmospheric pressure, eliminating the need for a vacuum chamber. Because of this characteristic, CAP is particularly suitable for treating aqueous solutions that contain heat-sensitive biological targets, including cells and their components.<sup>7–12</sup>

The ultimate goal is to optimize the utilization of reactive species for processing functional biological and chemical liquids in diverse applications. These include CAP-assisted drug discovery for the treatment of challenging diseases (e.g., cancer, autoimmune disorders, and genetic conditions); materials engineering and surface modification; and food engineering and preservation through antimicrobial action, contaminant removal, and functionalization (see ref. 11 and references therein).

In treating liquids with CAP, achieving uniform liquid treatment (ULT) is of utmost importance. However, existing systems and methods face significant hurdles due to the complex physical and chemical nature of plasma–liquid interactions.<sup>11–17</sup> For example, the patented Plasma-induced Modification of Biomolecules (PLIMB) technology<sup>18–22</sup> is an innovative CAP-assisted hydroxyl radical protein footprinting technique. It utilizes CAP to generate OH radicals for radical-probe mass spectrometry analysis of high-order protein structures.<sup>23–27</sup>

However, OH radicals, which are short-lived RONS, predominantly localize at the plasma–liquid interface, which limits

<sup>a</sup> Department of Electrical and Computer Engineering, University of Wisconsin-Madison, Madison, Wisconsin, 53706, USA. E-mail: hn4gg@missouri.edu

<sup>b</sup> Department of Surgery, University of Wisconsin-Madison, Madison, Wisconsin, 53706, USA

<sup>c</sup> Department of Animal and Dairy Sciences, University of Wisconsin-Madison, Madison, Wisconsin, 53706, USA

<sup>d</sup> Department of Biochemistry, University of Wisconsin-Madison, Madison, Wisconsin, 53706, USA

<sup>e</sup> Department of Biomedical Engineering, University of Wisconsin-Madison, Madison, Wisconsin, 53706, USA

<sup>f</sup> Carbone Cancer Center University of Wisconsin-Madison, Madison, Wisconsin, 53706, USA

<sup>g</sup> Charles W. Gehrke Proteomics Center, University of Missouri-Columbia, Columbia, Missouri, 65201, USA

<sup>h</sup> Materials Science and Engineering Institute, Department of Physics and Astronomy, University of Missouri Research Reactor (MURR), University of Missouri-Columbia, Columbia, Missouri, 65201, USA



their penetration into the bulk liquid.<sup>28</sup> In contrast, proteins and other biological targets requiring modification are distributed throughout the entire liquid volume. This mismatch often results in inadequate treatment in the bulk or excessive oxidation at the surface, leading to unintended modifications.<sup>23–27</sup> This is a well-known, long-lasting challenge in plasma–liquid interactions.

To date, methods aimed at achieving ULT have shown limited effectiveness. This limitation arises from the complex nature of liquid samples, their dynamic plasma interfaces, and the inherent variability in plasma parameters.<sup>29–32</sup> Two main strategies have been proposed:<sup>29–32</sup> (1) generating plasma directly in the bulk of the liquid, and (2) encapsulating plasma within gas bubbles formed at the nozzle exit of a plasma jet when the jet is submerged in the liquid. In the latter case, the plasma exists in the gas phase (inside a bubble) rather than in the liquid phase.

Both approaches face significant challenges.<sup>32</sup> The first risks overheating biological targets due to heat generated by plasma within the liquid.<sup>29,30</sup> The second suffers from the short lifespan and instability of plasma bubbles, which causes energy dissipation, bubble collapse, local heating, and mechanical agitation that can disrupt protein structure.<sup>31,32</sup>

Here, we address the persistent challenge of achieving ULT with CAP by exploring gas bubble mixing.<sup>33</sup> By controlling bubble formation in a single-bubble mode, each rising bubble generates a gentle laminar wake that enhances ULT while maintaining CAP stability.

To clarify the distinction of our approach, it is useful to compare it with prior strategies. Plasma bubbles generated within the liquid can improve reactive species penetration, but their effectiveness is limited by short lifetimes and instability, resulting in inconsistent treatment and localized heating upon collapse.<sup>31,32</sup> Some approaches exploit turbulent hydrodynamics of bubble-rise regimes, such as jetting, to intensify plasma–liquid interactions by increasing gas flow. However, this often drives the system into unstable turbulent conditions and imposes severe mechanical stress that can denature proteins and disrupt biomolecules.<sup>44–46</sup> Other mixing-enhancement methods, such as vigorous stirring or external agitation, can achieve bulk mixing but subject fragile biological targets to damaging hydrodynamic forces.<sup>34</sup>

In contrast, our method uses the controlled hydrodynamics of a single-bubble rise to generate a gentle, axisymmetric laminar wake. This wake promotes predictable and uniform liquid mixing without destabilizing the plasma or damaging sensitive molecules. This dual achievement—plasma stability and treatment uniformity—distinguishes our approach from previous plasma-bubble and mixing strategies.

Our proof-of-concept experiments demonstrate improved ULT by applying CAP generated *via* the PLIMB technology.<sup>18–22</sup> We tested various liquid samples containing organic molecules, including pH indicators, fluorescent probes for OH radicals, and proteins. This approach further enables rapid and efficient molecular modification, reducing the required CAP treatment time. Looking ahead, our results establish a general pathway for

CAP-assisted processing of functional material systems—such as exosomes, micelles, and surface-engineered nanoparticles—in aqueous suspension. We anticipate that these findings will inspire future research at the intersection of plasma physics, fluid dynamics, biomaterials, and chemical engineering, fostering the development of next-generation plasma-based materials processing technologies.

## 2. Results

This section presents the outcomes of our proof-of-concept experiments. The experiments were conducted on an integrated gas bubble mixing plasma reactor, as depicted in Fig. 1A.

### 2.1. Controlled hydrodynamics of spherical bubbles in distilled water using a low gas-flow rate

Fig. 2 presents sequential snapshots of bubble formation, rise, and break-up in a 1 mL volume of distilled water. The height of the water column is 10 mm. The top surface of the water volume interacts with either neutral humid air (Fig. 2A) or partially ionized air. In the latter case, CAP is generated in humid air above the water surface (Fig. 2B).

When no CAP is present on the water surface (plasma off, Fig. 2A), the single-bubbling regime follows a distinct progression. During the first 10 milliseconds ( $0 < t < 10$  ms, image 1), water rises up the microcapillary due to capillary attraction. Accumulating gas in the capillary develops sufficient pressure to push water down to the capillary orifice (see arrow in image 1). By  $t = 10$  ms (image 2), the first bubble, bubble 1, forms at the orifice, rapidly expands, and prepares to detach for its rise.

During the second 10 milliseconds ( $10 < t < 20$  ms, image 3), multiple dynamic events occur involving bubble 1 and

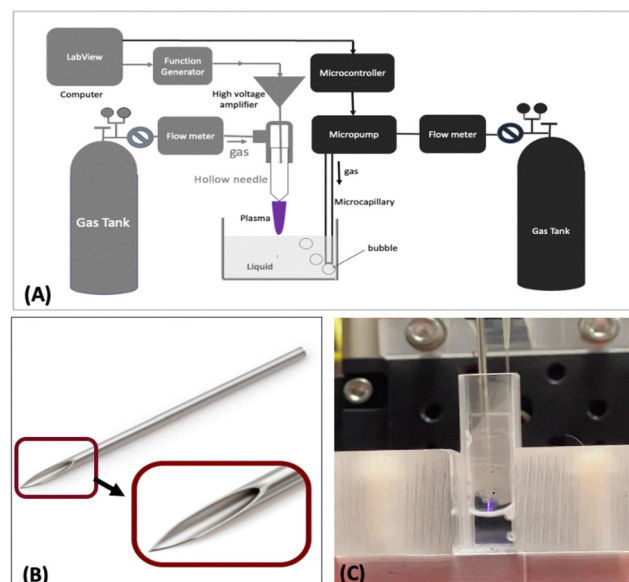


Fig. 1 The integrated system of PLIMB and gas bubble mixing to improve the treatment uniformity of liquid exposed to CAP. (A) Schematic of the integrated system, (B) an image of the hollow needle, (C) A cuvette containing liquid treated with CAP while being mixed using gas bubbles.



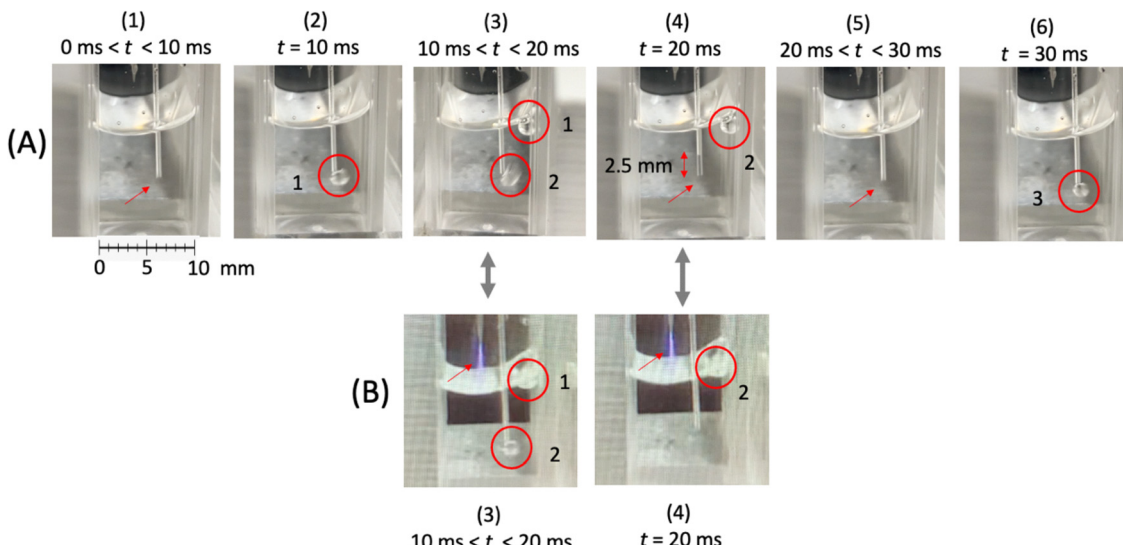


Fig. 2 Gas-bubble formation, rise, and break-up in a gas-plasma-liquid system controlled by injecting air into a submillimeter microcapillary with a sufficiently low gas-flow rate using a diaphragm micropump. (A) plasma is off, and (B) plasma is on. All images have the same spatial scale.

bubble 2. Bubble 1 rises to the water surface and breaks up (figuratively, its “death”). Simultaneously, bubble 2 forms at the orifice (its “birth”) and prepares to rise. Just before bubble 2 reaches the surface, bubble 1 breaks up ( $t = 20$  ms, image 4), creating space for bubble 2 to temporarily reside before its own breakup.

The dynamic events during the second 10-ms period play a crucial role in the behavior of bulk water and the plasma–liquid interface. However, they do not impact plasma stability. This is evident in images 3 and 4 of Fig. 2B, where bubbling occurs in the presence of CAP.

Returning to Fig. 2A, it is also noted that as the diaphragm of the micropump relaxes and the gas in the microcapillary loses pressure, a water column (approximately 2.5 mm in height) reappears at the lower part of the microcapillary due to capillary attraction (see the arrow pointing to the orifice in image 4). After this relaxation, the cycle repeats, as seen in images 5 and 6 of Fig. 2A for  $t > 20$  ms; another (bubble 3) is newly formed, and the sequence continues periodically.

## 2.2. Enhanced CAP liquid treatment uniformity using gas bubble mixing

To evaluate the effectiveness of gas-bubble mixing in improving the uniformity of liquid treatment with CAP, we employed two complementary methods—a qualitative colorimetric indicator and a semi-quantitative fluorescence probe. Together, they allow visual and analytical assessment of treatment uniformity with and without gas bubble mixing.

**2.2.1. Qualitative measure using a pH indicator.** A qualitative measure was obtained using *bromophenol blue*, a pH indicator dissolved in distilled water. This dye exhibits a distinct color transition from blue ( $\text{pH} > 4.6$ ) to yellow ( $\text{pH} < 3$ ), thereby visually mapping the spatial distribution of acidification caused by RONS generated by CAP. The objective of this experiment was to qualitatively examine the pH change of water due to CAP-induced

long-lived species (e.g.,  $\text{NO}_2^-$  and  $\text{NO}_3^-$ ) that correspond to acids such as  $\text{HNO}_2$  and  $\text{HNO}_3$  traversing the plasma–liquid interface and entering the bulk water.

It should be emphasized that although  $\text{NO}_2^-$  and  $\text{NO}_3^-$ , similar to  $\text{H}_2\text{O}_2$ , are key long-lived RONS typically generated in plasma–liquid systems, they are not the primary focus of this study. Instead, the experiments with bromophenol blue were carried to investigate the propagation and spatial distribution of acidity within a distilled water column contained in a cuvette. The objective is to demonstrate the effectiveness of bubble-induced mixing in achieving a uniform dispersion of acidic groups (including, but not limited to,  $\text{NO}_2^-$  and  $\text{NO}_3^-$ ) throughout the liquid volume treated by CAP. Moreover, as will be seen in this Results section, because distilled water possesses only a limited buffering capacity against plasma-induced acidification, phosphate-buffered saline (PBS) is employed in this work as the working liquid to dissolve terephthalic acid and myoglobin, thereby maintaining pH stability during CAP treatment—an essential factor for, for instance, preserving the native conformation of proteins in aqueous environments. Finally, the ultimate goal of this work is to advance the PLIMB technology, which, as described in the Introduction, leverages OH radicals generated through plasma–liquid interactions as a novel hydroxyl radical footprinting technique for radical-probe mass spectrometry proteomics. This enables structural analysis of high-order protein conformations and protein–protein interactions. Therefore, rather than focusing on  $\text{H}_2\text{O}_2$ ,  $\text{NO}_2^-$ , or  $\text{NO}_3^-$ , this study primarily concentrates on how to improve the uniform distribution of OH radicals in chemical and biological liquids such as PBS.

The snapshots in Fig. 3 provide sequential, real-time observations of the CAP treatment process applied to a 30-mm dye column. As shown in Fig. 3A, in the absence of gas-bubble mixing, the color change to yellow remains confined to a thin surface layer ( $\sim 10$  mm) even after 30 s of treatment, indicating



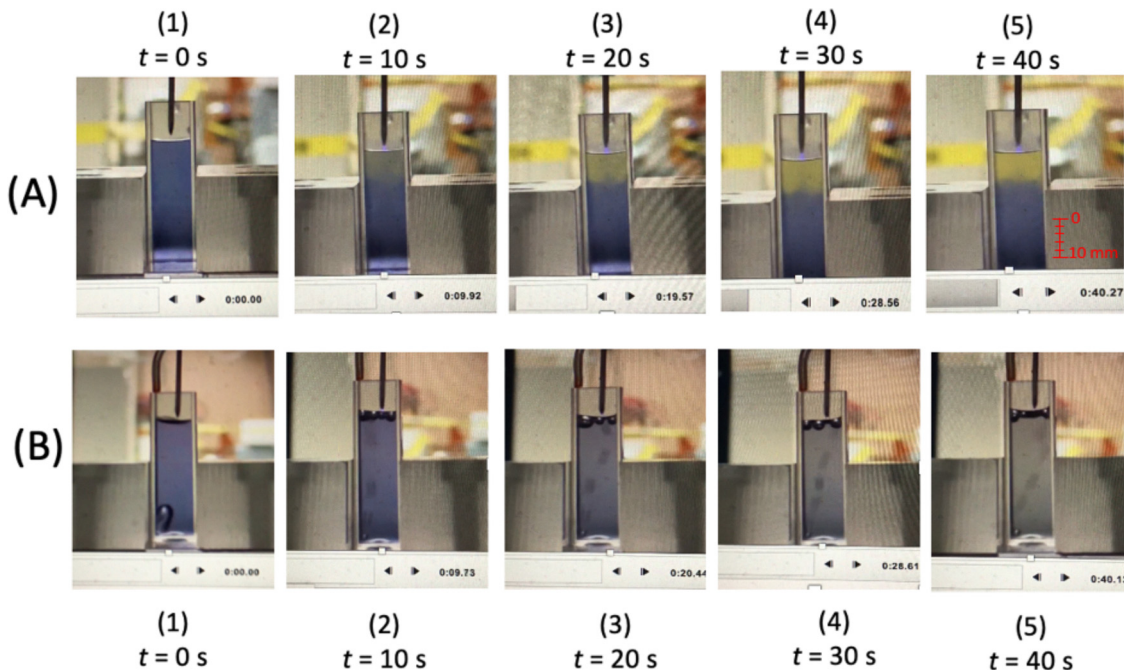


**Fig. 3** Alteration of the pH value of the solution of bromophenol blue dye dissolved in distilled water treated with CAP (A) without and (B) with gas bubble mixing. The blue and yellow colors indicate the less-acidic pH values ( $\text{pH} > 4.6$ ) (blue) and more-acidic pH values ( $\text{pH} < 3$ ) (yellow) ( $\text{pH} < 3$ ), respectively. All images have the same spatial scale.

poor penetration of reactive species. In contrast, with gas-bubble mixing (Fig. 3B), the yellow coloration becomes uniformly distributed throughout the 30-mm liquid column within 20 s, demonstrating significantly enhanced mixing and homogeneous treatment. The dimmer yellow hue observed under gas bubble mixing [see panels (4) and (5) of Fig. 3B] reflects a more uniform, diluted distribution of acidic species throughout the liquid rather than excessive local accumulation near the surface. This color change thus serves as a qualitative indication of improved treatment uniformity.

**2.2.2. Semi-quantitative measure using terephthalic acid fluorescence.** To semi-quantitatively assess the efficacy of the gas-bubble mixing method, experiments were performed using terephthalic acid (TA) as a fluorescent probe for OH radicals produced during CAP treatment, with and without gas bubble mixing. As aforementioned, the working liquid was PBS solution at pH 7.4. CAP-generated OH radicals react with TA to form 2-hydroxyterephthalic acid (HTA), a stable fluorescent product with a known yield of 30–37% across a wide pH range (pH = 4 to pH = 10). The fluorescence intensity of HTA correlates with the cumulative OH radicals concentration in the liquid (the detailed description of this fluorescence dosimetry for OH radicals detection and optimization in plasma-liquid systems can be found in our previous work, ref. 58).

By comparing the fluorescence intensity of HTA in post-treated samples collected from the liquid surface and bottom, we can assess the degree of spatial uniformity of CAP treatment. The closer the fluorescence intensities between these two sampling depths, the greater the treatment uniformity achieved.

In the pre-treated solution (0.1 mM TA, 3 mL total volume), TA is uniformly distributed throughout the PBS solution. Consequently, the fluorescence values of 100  $\mu\text{L}$  samples collected from the surface and bottom are nearly identical, serving as the control at  $t = 0$  s, where  $t$  is the CAP treatment time. Based on the previous bromophenol blue experiments (Fig. 3), two treatment times ( $t = 20$  s and  $t = 40$  s) were selected for comparison.

As shown in Fig. 4A, without gas bubble mixing, the HTA fluorescence intensity at the liquid surface increases approximately 2.5-fold and 3.5-fold relative to the control after 20 and 40 s of CAP treatment, respectively. In contrast, fluorescence at the bottom increases only slightly (by 17% and 23%), indicating limited transport of OH radicals into the bulk and that oxidation occurs predominantly near the interface.

Conversely, Fig. 4B shows that when gas-bubble mixing is applied, the HTA fluorescence intensities of the surface and bottom samples become very close, differing by only 5.4% and 3.0% after 20 s and 40 s, respectively. This provides clear quantitative evidence that the gas-bubble mixing method effectively enhances uniformity when CAP is generated at the liquid surface.

It should be noted that although this TA experiment analytically demonstrates the effectiveness of gas bubble mixing, the percentage of TA modified by OH radicals is relatively high (40–65%), exceeding the ideal oxidation range (10–30%) typically required for hydroxyl radical protein footprinting in radical-probe mass spectrometry analysis of high-order protein structures and complexes.<sup>23–27</sup> To mitigate over-oxidation, the treatment time should be shortened. In the following section,



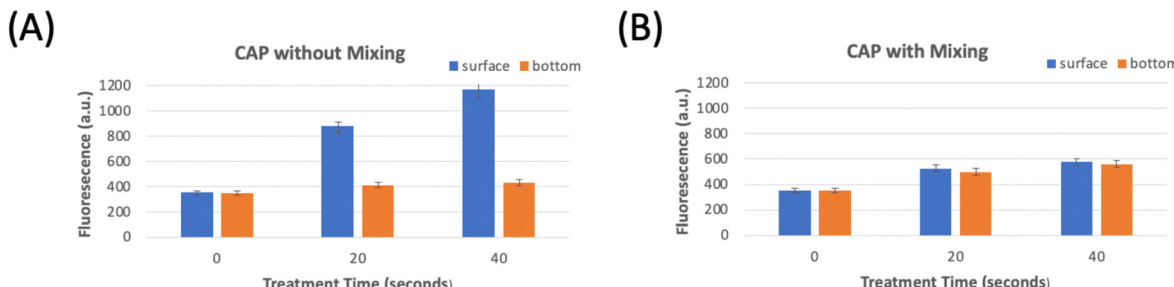


Fig. 4 The fluorescence of 2-hydroxy-terephthalic acid formed at the surface and bottom of phosphate-buffered solutions consisting of terephthalic acid that reacts with OH radicals after CAP treatment without (A) and with (B) using gas bubble mixing method for different treatment times.

myoglobin proteins are used as a model system to illustrate this effect.

**2.2.3. Summary.** These qualitative and semi-quantitative analyses together demonstrate that laminar gas bubble mixing substantially enhances the uniformity of CAP treatment in liquids, even without complex imaging instrumentation. Future studies will aim to establish fully quantitative uniformity metrics by integrating spatially resolved, position-sensitive fluorescence or optical imaging (*e.g.*, charge coupled device (CCD)-based color mapping) into the CAP–liquid reactor to monitor pH color indication of bromophenol blue or HTA fluorescence gradient in real time.

### 2.3. Accelerated CAP treatment using gas bubble mixing

This subsection aims to demonstrate the efficacy of the gas bubble mixing approach in accelerating CAP treatment for biological samples, particularly those containing oxidation- and heat-sensitive substances such as proteins. We utilize a pH-buffering bovine oxy-myoglobin solution at a concentration of 5  $\mu$ M and pH 6 as the biological-liquid model. In the presence of excessive oxygen and nitrogen species, including OH radicals and hydrogen peroxide, oxy-myoglobin in its +2-oxidation state can undergo activation and form ferryl-myoglobin species (either the Fe(IV)=O state or Fe(IV)=O radical state).<sup>35–37</sup> These species have the potential to catalyze lipid peroxidation, resulting in the deterioration of meat quality (*e.g.*, meat discoloration and off-flavor development).<sup>35–37</sup> Moreover, the formation of ferryl-myoglobin species may have implications for ischemia/reperfusion injury, characterized by abrupt cellular destruction in cardiac and skeletal muscle tissues.<sup>38</sup> Therefore, a comprehensive understanding and control of myoglobin oxidation mechanisms is also vital for healthcare applications.<sup>39,40</sup>

Our previous research has revealed that CAP generation using the PLIMB technology in combination with radical-probe mass spectrometry can serve as a platform to enhance our understanding of the oxidation of myoglobin and hemoglobin.<sup>41</sup> However, the lack of uniform and efficient treatment, which was performed without the aid of the gas bubble mixing method, has limited the analysis and interpretation of mass spectrometry data obtained from CAP-treated myoglobin samples. Here, we compare CAP treatment of myoglobin with and without gas bubble mixing, demonstrating that

this approach can overcome these challenges and improve quality control while reducing treatment time.

The design of this experiment was based on our previous findings regarding pH alteration in bromophenol blue dye (as discussed in Section 2.2.1). This experiment focuses on a 10-mm column of oxy-myoglobin solution, which is as high as the yellow-colored acidic surface region of the dye liquid shown in Fig. 3A (image 5,  $t = 10$  s), for CAP treatment. We compared treatments with and without gas bubble mixing. The hydrodynamics of this system were well-controlled, similar to the previously described case using distilled water (Section 2.1) since the protein was very dilute (5  $\mu$ M) that it was of low viscosity (see Discussion section for thorough insights). Treatment times were carefully chosen in the range of 0 to 4.5 s, as shown in Fig. 5, which illustrates the percentage of ferryl-myoglobin formed as a function of the treatment duration.

The results clearly demonstrate that gas bubble mixing improves treatment uniformity and significantly reduces treatment time. For instance, to achieve 10% ferryl-myoglobin through oxy-myoglobin oxidation, the estimated treatment time can be reduced from 3 seconds to 1.5 seconds by incorporating gas bubble mixing, thus doubling the treatment efficiency. This accelerated treatment could mitigate the potential risks associated with excessive

### Oxymyoglobin Oxidation in CAP Treatment

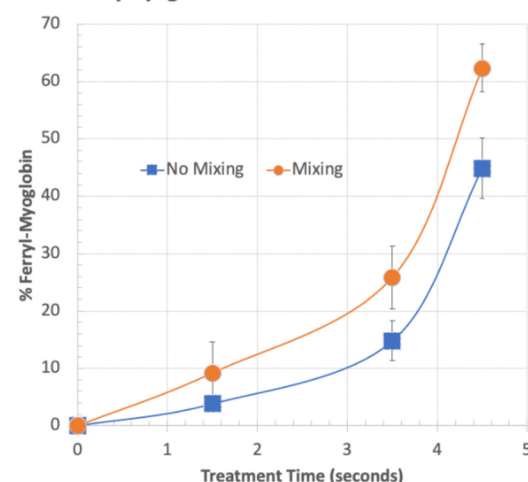


Fig. 5 Oxymyoglobin oxidation to Ferryl-Myoglobin in CAP treatment with and without gas bubble mixing.



oxidation damage or unintended modifications to protein samples. In addition, decreasing the treatment time is economically critical in the plasma-processing industry, where the throughput can be increased. This is the objective that commercialized CAP systems such as the PLIMB technology aims at for its increased demand service for the growing protein-based therapeutic market.

### 3. Discussions

The outcomes of these proof-of-concept experiments support our central hypothesis that the hydrodynamics of bubbles in liquid can be effectively controlled to achieve gentle laminar wakes as an effective mixing mechanism that improves liquid treatment without jeopardizing plasma stability (see Fig. 6). To gain further insights into our approach, we discuss the key aspects of hydrodynamics of single-bubble formation and rise in liquid.

In gas-liquid systems involving gas bubbles, bubble formation plays a crucial role in subsequent dynamic processes such as bubble rise, coalescence, and breakup.<sup>33</sup> The wake formed immediately behind a rising bubble contains a portion of liquid along with dissolved substances, including solid particles like molecular solutes, particulate substances like nanoparticles, biological cells, and their components, all of which are treated as a solid phase to distinguish them from the liquid phase (solvent), and gas phase (bubbling gas) as shown in Fig. 6. This wake induces liquid mixing through two primary mechanisms: solid circulation and solid exchanges. The details

of these mechanisms were discussed in ref. 42, a short description is given here. Solid circulation involves the entrapping of solids in the wake of the bubble formed at the orifice near the liquid bottom, transport to the top, deposition on the liquid surface, and subsequent circulation back down to the bottom. Solid exchanges occur as some solids are exchanged between the bubble wake and the emulsion phase underneath of the bubble's ascent.<sup>42,43</sup> The dynamics of the wake strongly depend on the bubble formation regimes.<sup>44,45</sup>

The Reynolds number ( $Re$ ), defined as the dimensionless ratio of inertial and viscous forces ( $Re = 4Q/\pi\nu D$ , where  $Q$  is the volumetric flow rate,  $\nu$  is the kinematic viscosity of the gas, and  $D$  is the inner diameter of the microcapillary), serves as a predictive factor for fluid behavior, including flow patterns such as laminar and turbulent flows. It can be effectively utilized as a control parameter<sup>44–48</sup> to dynamically determine various bubble formation regimes, ranging from single bubbling ( $Re < 170$ ) to jetting ( $Re > 12\,000$ ).<sup>45</sup> By controlling the flow rate ( $Q$ ) of bubbling gas (with fixed  $\nu$ ) through the microcapillary (with fixed  $D$ ), one can control the Reynolds number.<sup>45–49</sup> For example, if  $\nu = 1.0 \times 10^{-6} \text{ m}^2 \text{ s}^{-1}$  and  $D = 0.3 \text{ mm}$ , then  $Re \approx 70.7Q$ , given that  $Q$  was measured in  $\text{mL min}^{-1}$ . A simplified schematic summarizing bubble regime transitions with increased Reynold number and flow rate is shown in Fig. 7.

The dynamic events observed in Section 2.1 (see Fig. 2) are commonly observed in the liquids when subjected to sufficiently low gas-flow rates within the single-bubbling regime.<sup>45</sup> In this regime, spherical and monodispersed bubbles are formed, followed by an individual rise and an irregular

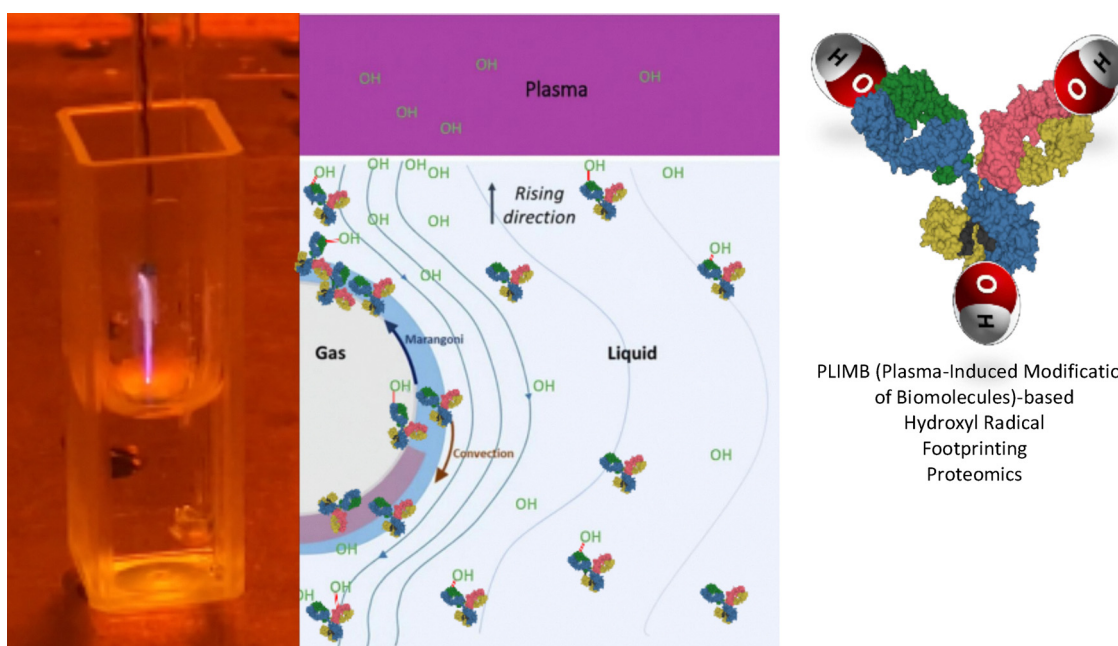


Fig. 6 Gas bubble mixing induced by the controlled laminar wake of a rising single bubble, providing an alternative approach to improve the uniformity of liquid treatment in cold atmospheric plasma (CAP) processes—one of the major challenges in plasma–liquid interactions. This bubble-driven mixing strategy can enhance plasma-based technologies, such as Plasma-induced Modification of Biomolecules (PLIMB), enabling precise hydroxyl radical footprinting of proteins and the study of protein–protein interactions, thereby accelerating drug discovery for protein-based therapeutics.



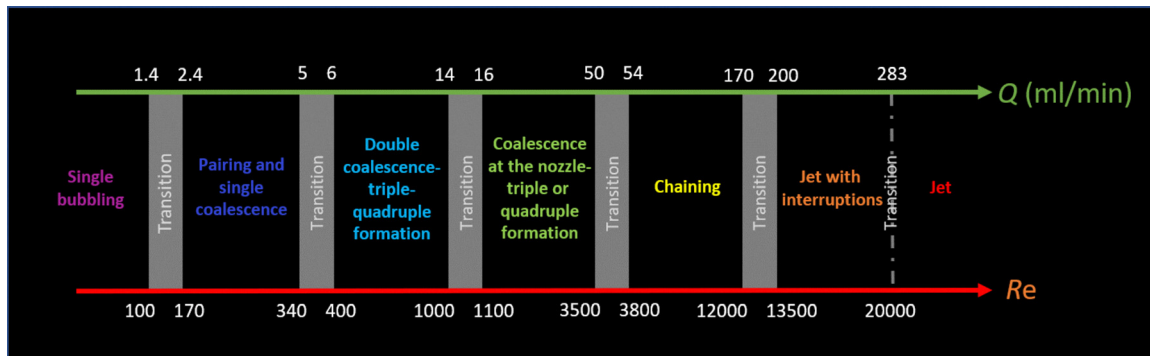


Fig. 7 Schematic for the transitions among different bubbling regimes from single bubbling ( $Re < 170$  and  $Q < 2.4 \text{ mL min}^{-1}$ ) to jetting ( $Re > 1200$  and  $Q > 170 \text{ mL min}^{-1}$ ). The names of the bubbling regimes were given by Kyriakides *et al.* in ref. 45.

deformation upon detachment from the microcapillary orifice. The hydrodynamics governing these processes are consistent and repetitive, with a fixed period of approximately 20 milliseconds. Importantly, this controlled hydrodynamics condition generates a gentle axisymmetric laminar wake that effectively mixes the liquid without any discernible impact on the subsequent formation of bubbles.<sup>32,45,50–52</sup>

According to the analyses of Kulkarni *et al.*<sup>33</sup> and Sadhal *et al.*,<sup>43</sup> bubble size, Reynolds number (*i.e.*, volumetric gas flow rate), and the resulting hydrodynamic wake strongly influence the transport of plasma-generated reactive species. Smaller bubbles, typically around 1.5–2.0 mm in diameter, provide a higher surface-area-to-volume ratio, thereby promoting efficient transfer of organic molecules such as terephthalic acid (TA) and myoglobin from the bulk liquid to the plasma–liquid interface, where OH radicals are primarily produced and react these molecules. Maintaining a low Reynolds number ensures laminar, axisymmetric wakes that facilitate predictable transport and homogeneous distribution of RONS as well as chemical and biological targets throughout the liquid. In contrast, turbulent wakes at higher Reynolds numbers can exert excessive mechanical forces that disrupt folded protein structures and destabilize the plasma. The gentle laminar wakes generated under controlled single-bubble conditions, as demonstrated in this work, enable uniform CAP treatment of chemical (*e.g.*, TA) and/or biological (*e.g.*, myoglobin) targets in their liquids, thereby delivering the uniformity of CAP reactivity throughout the whole volume of the CAP-treated liquids while minimizing perturbations that could compromise plasma–liquid interactions and experimental reproducibility. Further theoretical and experimental efforts are anticipated to deepen our understanding of these effects.

Furthermore, the dimensions and top submergence of the capillary, together with the selected gas-flow rate, were carefully optimized to generate bubbles with diameters of approximately 1.5–2.0 mm in the low-viscosity liquids investigated in this study.<sup>44,53,54</sup> These results are consistent with the work of Siemes and Kaufmann,<sup>54</sup> who demonstrated that, under low gas-flow conditions in low-viscosity media, the volume difference between spherical bubbles formed at specific flow rates and those formed at infinitesimally small flow rates using the

same orifice remains independent of liquid viscosity, surface tension, and density. Maintaining such small bubbles is also critical to suppress jetting phenomena,<sup>55</sup> in which bursting bubbles at the liquid surface eject liquid droplets into the surrounding air,<sup>55,56</sup> thereby disturbing plasma stability. Collectively, these findings confirm that precise control of gas-flow rate and bubble hydrodynamics enables the formation of uniform, laminar, and predictable wakes that act as an effective mixing mechanism to improve the uniformity and reproducibility of plasma–liquid treatment—outcomes that remain challenging to achieve with transient, unstable plasma bubbles traditionally formed in liquids.<sup>31,32</sup>

In conclusion, the controllable gas bubble mixing approach presented here offers a robust and scalable method for treating chemical and biological liquids containing sensitive substances such as proteins. Unlike traditional techniques,<sup>29–32</sup> which either risk overheating the targets when generating plasma in the bulk liquid<sup>29,30</sup> or suffer from the short lifespan and instability of plasma bubbles,<sup>31</sup> this method provides controlled and uniform treatment by precisely managing bubble hydrodynamics. The approach ensures gentle yet effective liquid mixing without compromising plasma stability, enhancing treatment uniformity and reducing processing time. Importantly, the method is inherently adaptable for scaling up, enabling its integration into larger-volume systems required in industrial plasma-assisted processing. These features make it a promising platform for applications in food safety, therapeutic product manufacturing, and healthcare, where nonthermal plasma treatment of aqueous biological samples is critical. Prospectively, the combination of controlled bubble dynamics and cold plasma could enable continuous-flow processing, high-throughput sample treatment, and precise modulation of reactive species, opening avenues for commercial and clinical adoption of plasma-based technologies.<sup>59–63</sup>

## 4. Experiments

### Systems

Our system of bubble-mixing CAP reactor is described in this section. Within the setup that is depicted in Fig. 1, a crucial



element is the CAP-generated subsystem employing patented PLIMB technology (commercialized by Immuno Scientific), which has been extensively characterized in previous studies<sup>18–22</sup> including detailed analysis of the generation of OH radicals as the key RONS of primary interest in this work. Controlled by a LabVIEW program, a function generator (HP/Agilent 8116A model) supplies an AC voltage sinusoidal signal to a high-voltage amplifier (Trek 10/40A-HS model), which amplifies the signal by a factor of a thousand. This amplified signal powers a stainless-steel hollow needle (Fig. 1B) functioning as a high-voltage electrode, generating a CAP using ambient air in the laboratory environment served as the working gas instead of flowing gas through the needle. It should be noted that while our setup in Fig. 1 is equipped with the hollow needle that can, in principle, deliver gas to the discharge region, this functionality was not used in the current study. Future research will extend current work to study the effects of different working gases (either for generating CAP or the single bubble) and associated flowing rates on the single bubble hydrodynamics, the mixing efficacy, and the chemistry of the plasma-liquid system.

The voltage amplitude is set at 7.5 kV, and the frequency is fixed at 10 kHz. The liquid under investigation is contained in a UV-transmitting cuvette, with its wall acting as a dielectric barrier. The cuvette is thermally connected to a grounded metallic cooler (Peltier cooler), serving as both the grounded electrode and the heat bath for the reactor.

Another critical component is the gas bubble mixing subsystem (Fig. 1A), that is designed based on knowledge of various gas-liquid systems involving gas bubbles. A top-submerged microcapillary is utilized to introduce air or other feed gas into the liquid in the cuvette. It has an outer diameter of 0.5 mm, an inner diameter of 0.3 mm, and a length of 40 mm. The air is introduced using a diaphragm micropump (KNF NMP 03 KPDC-L model) at a precisely controlled volumetric gas-flow rate, which is maintained at a sufficiently low level of  $1.0 \text{ mL min}^{-1}$  to ensure bubble formation occurs within the single-bubbling regime.

## Materials

The aqueous solutions in this study exhibit low viscosity and are treated as inviscid and incompressible liquids. The first liquid is distilled water, specifically the Milli-Q EQ 7000 ultra-pure water with a resistivity of  $18.2 \text{ M}\Omega \text{ cm}$  at  $25^\circ\text{C}$ . The second liquid is 0.04 wt% bromophenol blue ( $\text{C}_{19}\text{H}_9\text{Br}_4\text{NaO}_5\text{S}$ ) dissolved in water (Sigma, CAS # 34725-61-6). This solution serves as a pH indicator, appearing yellow for  $\text{pH} < 3$  and blue for  $\text{pH} > 4.6$ . The third liquid is terephthalic acid,  $\text{C}_6\text{H}_4(\text{CO}_2\text{H})_2$  (Sigma, CAS # 100-21-0), dissolved at a concentration of 0.1 mM in 1% phosphate buffered saline (1× PBS) at  $\text{pH} 7.4$ . The last liquid is bovine oxymyoglobin, dissolved at a concentration of 5  $\mu\text{M}$  in sodium phosphate (100 mM) at  $\text{pH} 6$ .

## Methods

Videos from which the images in Fig. 2 and 3 were extracted were recorded using an iPhone SE (2022) camera at 240 frames per second. The recorded videos were converted into sequentially

ordered snapshots for analysis. In the experiments shown in Fig. 4, 1 mL aliquots of liquid containing 0.5 mM terephthalic acid in 1× PBS were pipetted into individual cuvettes for CAP treatment, both with and without gas-bubble mixing. Immediately after each treatment, the cuvette was kept stationary; the treated liquid was not disturbed or mixed. Subsequently, 100  $\mu\text{L}$  of post-treated liquid was sampled from both the liquid surface and the bottom using a pipette, and each sample was transferred into separate wells of a 96-well plate for fluorescence measurement. Fluorescence was recorded at an excitation wavelength of 310 nm and an emission wavelength of 425 nm using a FlexStation® 3 multi-detection microplate reader. Each treatment was performed in eight replicates, and fluorescence data were averaged to obtain mean values, with standard deviations represented as error bars in Fig. 4.

For the data presented in Fig. 5, the CAP-treated 5  $\mu\text{M}$  myoglobin solutions were gently mixed with a pipette immediately after each treatment, and 1 mL aliquots were taken for subsequent analysis. The absorption spectra of the post-treated samples were then measured using a UV-Vis spectrophotometer (Shimadzu UV-2600) over the wavelength range of 400–700 nm. Each data point in Fig. 5 represents the mean  $\pm$  standard deviation from three replicates. The post-treated solutions contained three dominant myoglobin species—oxymyoglobin (Oxy-Mb), metmyoglobin (Met-Mb), and ferryl-myoglobin (ferryl-Mb)—whose concentrations were determined using the well-established Jourd'heuil equations<sup>57</sup> based on absorbance values at 490, 560, and 580 nm. The ferryl-Mb fraction was then calculated as a percentage and averaged over three replicates, with the resulting mean and standard deviation plotted as a function of treatment time in Fig. 5.

## Statistics analysis

All experiments were replicated independently: TA fluorescence measurements (Fig. 4) were performed in  $n = 8$  independent replicates, and myoglobin oxidation assays (Fig. 5) were performed in  $n = 3$  biological/technical replicates (see Experiments for sampling details). Data are reported as mean  $\pm$  standard deviation (SD) and plotted with SD error bars. For comparisons of fluorescence intensities between the surface and bottom samples collected from the same treated cuvette (Fig. 4), we used a two-tailed paired Student's *t*-test, since surface and bottom samples were paired within the same experimental run. For comparisons of ferryl-myoglobin percentages between treatments with and without bubble mixing at matched timepoints (Fig. 5), we used a two-tailed unpaired Student's *t*-test assuming unequal variances (Welch's correction) unless equal variances were confirmed by an *F*-test. The results show that the difference between surface and bottom fluorescence intensities under gas-bubble-mixed conditions is not statistically significant ( $p > 0.05$ ), indicating improved uniformity, while the difference is statistically significant ( $p < 0.05$ ) without bubble mixing, consistent with our hypothesis.

## Conflicts of interest

The authors claim no conflict of interest.



## Data availability

The datasets supporting the findings of this study are available from the corresponding author upon reasonable request.

## Acknowledgements

This project was fully funded to H. D. L by the American Pediatric Surgical Association's Jay Grosfeld Scholar Grant and by the University of Wisconsin School of Medicine and Public Health Department of Surgery's Research Fund. This project was also partially supported by the U.S. Federal Government under Federal Grant No. 2019-67017-29179 awarded by the U.S. Department of Agriculture, Federal Grant No. 2019-67017-29179 awarded by the U.S. Department of Agriculture's National Institute of Food and Agriculture, Federal Grant No. 2010789 and 1943816 awarded by the U.S. National Science Foundation, and Federal Grant No. DE-FG02-88ER13938 awarded by the U.S. Department of Energy (Office of Basic Energy Sciences, Division of Chemical Sciences, Geosciences, and Biosciences). This work was also partially supported by a gift fund generously provided to M. R. S. via the University of Wisconsin-Madison by the Susan and Chris Salm Foundation. H. M. N. would like to acknowledge his Postdoctoral Fellowship and seeking research fund (Grant No. CD002339) awarded by the Materials Science and Engineering Institute, the University of Missouri, Columbia, Missouri. H. M. N. would also like to express his appreciation to the profound discussions of the potential of the future scientific and technological impacts of this work with the CEO (Dr. Faraz A. Choudhury) and the CTE (Dr. Daniel Benjamin) of Immuto Scientific (Madison, Wisconsin, USA), and with a Principal Scientist (Dr. Bindu Nair) of Eurofins BioPharma Product Testing North America (Columbia, Missouri, USA). Myoglobin was generously provided to M. P. R. by Prof. Surendranath P. Suman at the University of Kentucky.

## References

- 1 Z. Chen and R. E. Wirz, *Cold Atmospheric (CAP) Technology and Applications*, 2021, Morgan and Claypool.
- 2 M. Laroussi, *Cold Plasma in Medicine and Healthcare: The new Frontier in Low Temperature Plasma Applications*, *Front. Phys.*, 2020, **8**, 74.
- 3 *Low Temperature Plasma Technology: Methods and Applications*, ed. P. K. Chu and X. Lum, CRC Press, 2020.
- 4 X. Lu, S. Reuter, M. Laroussi and D. Liu, *Nonequilibrium Atmospheric Pressure Plasma Jets: Fundamentals, Diagnostics, and Medical Applications*, CRC Press, 2019.
- 5 A. Fridman and L. A. Kennedy, *Plasma Physics and Engineering*, CRC Press, 3rd edn, 2016.
- 6 M. Keidar and I. Beilis, *Plasma Engineering*, Elsevier Science, 2nd edn, 2018.
- 7 S. Samukawa, *et al.*, The 2012 Plasma Roadmap, *J. Phys. D: Appl. Phys.*, 2012, **45**, 253001.
- 8 I. Adamovich, *et al.*, The 2017 Plasma Roadmap: Low Temperature Plasma Science and Technology, *J. Phys. D: Appl. Phys.*, 2017, **50**, 323001.
- 9 I. Adamovich, *et al.*, The 2022 Plasma Roadmap: Low Temperature Plasma Science and Technology, *J. Phys. D: Appl. Phys.*, 2017, **50**, 323001.
- 10 X. Lu, P. J. Bruggeman, S. Reuter, G. Naidis, A. Bogaerts, M. Laroussi, M. Keidar, E. Robert, J. M. Pouvesle, D. Liu and K. Ostrikov, Grand Challenges in Low Temperature Plasmas, *Front. Phys.*, 2022, **10**, 1040658.
- 11 P. J. Bruggeman, *et al.*, Plasma-liquid interactions: a review and roadmap, *Plasma Sources Sci. Technol.*, 2016, **25**, 053002.
- 12 L. Gao, X. Shi and X. Wu, Applications and Challenges of Low Temperature Plasma in Pharmaceutical Field, *J. Pharm. Anal.*, 2021, **11**, 28–36.
- 13 S. B. Ebrahimi and B. Samanta, Engineering Protein-based Therapeutics Through Structural and Chemical Design, *Nat. Commun.*, 2023, **14**, 2411.
- 14 *Plasma Chemistry and Catalysis in Gases and Liquids*, ed. V. I. Parvulescu, M. Magureanu and P. Lukes, Wiley-VCH Verlag & Co. KGaA, 2012.
- 15 F. Rezaei, *et al.*, Applications of Plasma-Liquid Systems: Review, *Materials*, 2019, **12**, 2751.
- 16 P. Viegas, E. Slikboer, Z. Bonaventura, O. Guaitella, A. Sobota and A. Bourdon, Physics of plasma Jets and Interaction with Surfaces: Review on Modelling and Experiments, *Plasma Sources Sci. Technol.*, 2022, **31**, 053001.
- 17 U. Kogelschatz, B. Eliasson and W. Egli, Dielectric-Barrier Discharges: Principle and Applications, *J. Phys. IV*, 1997, **07(C4)**, C4–47.
- 18 Michael R. Sussman, J. Leon Shohet, Faraz A. Choudhury, Joshua M. Blatz, Benjamin B. Minkoff and Daniel I. Benjamin, Methods, Systems, and Compositions for Studying Solvent Accessibility and Three-dimensional Structure of Biological Molecules, *US Pat.*, 10571460, <https://www.osti.gov/doepatents/biblio/1632612>.
- 19 B. B. Minkoff, J. M. Blatz, F. A. Choudhury, D. Benjamin, J. L. Shohet and M. R. Sussman, Plasma-Generated OH Radical Production for Analyzing Three-Dimensional Structure in Protein Therapeutics, *Nat. Sci. Rep.*, 2017, **7**, 12946.
- 20 J. M. Blatz, D. Benjamin, F. C. Choudhury, B. B. Minkoff, M. R. Sussman and J. Leon Shohet, Effect of frequency and applied voltage of an atmospheric-pressure dielectric-barrier discharge on breakdown and hydroxyl-radical generation with a liquid electrode, *J. Vac. Sci. Technol. A*, 2020, **38**, 043001.
- 21 D. Benjamin, PhD thesis, Plasma-Generated Hydroxyl Radicals for Epitope Mapping, UW-Madison's Library, 2021.
- 22 J. Blatz, PhD thesis, The Effects of Electrical, Physical, and Chemical Parameters on a Dielectric Barrier Discharge with a Liquid Electrode, UW-Madison's Library, 2021.
- 23 A. McKenzie-Coe, *et al.*, Hydroxyl radical protein footprinting: a mass spectrometry-based structural method for studying the higher order structure of proteins, *Chem. Rev.*, 2022, **122**, 7532.
- 24 X. R. Liu, M. M. Zhang and M. L. Gross, Mass Spectrometry-based Protein Footprinting for High-order Structure Analysis: Fundamentals and Applications, *Chem. Rev.*, 2020, **27**, 4355.



25 D. T. Johnson, L. H. Di Stefano and L. M. Jones, Fast photochemical oxidation of proteins (FPOP): A powerful mass spectrometry-based structural proteomics tool, *J. Biol. Chem.*, 2019, **294**, 11969.

26 L. Konermann, S. Vahidi and M. A. Sowole, Mass Spectrometry Methods for Studying Structure and Dynamics of Biological Macromolecules, *Anal. Chem.*, 2014, **86**, 213.

27 S. D. Maleknia and K. M. Downard, Advances in Radical Probe Mass Spectrometry for Protein Footprinting in Chemical Biological Applications, *Chem. Soc. Rev.*, 2014, **43**, 3244.

28 S. Kim and C.-H. Kim, Applications of Plasma-Activated Liquid in the Medical Field, *Biomedicines*, 2021, **9**, 1700.

29 Y. Yang, Y. I. Cho and A. Fridman, *Plasma Discharge in Liquid: Water Treatment and Applications*, CRC Press, 2012.

30 S. Horikoshi and N. Serpone, In-liquid plasma: a novel tool in the fabrication of nanomaterials and in the treatment of wastewaters, *PRC Adv.*, 2017, **7**, 47196.

31 R. Hong, *et al.*, Plasma Bubbles: A Route to Sustainable Chemistry, *AAPPS Bull.*, 2021, **31**(16), 1–14.

32 W. Zhang, *et al.*, Review of bubble dynamics on charged liquid-gas flow, *Phys. Fluids*, 2023, **35**, 021302.

33 A. A. Kulkarni and J. B. Joshi, Bubble Formation and Bubble Rise Velocity in Gas-Liquid Systems: A Review, *Ind. Eng. Chem. Res.*, 2005, **44**, 5873.

34 J. Jaspe and S. J. Hagen, Do Protein Molecule Unfold in Simple Shear Flow?, *Biophys. J.*, 2006, **91**, 3413.

35 C. Wongwichian, S. Klomklao, W. Panpipat, S. Benjakul and M. Chaijan, Interrelationship between myoglobin and lipid oxidations in oxeye scad (Selar boops) muscle during iced storage, *Food Chem.*, 2015, **174**, 279.

36 C. P. Baron and H. J. Andersen, Myoglobin-Induced Lipid Oxidation. A Review, *J. Agric. Food Chem.*, 2002, **50**, 3887.

37 Jens K. S. Møller and Leif H. Skibsted, Myoglobins—the link between discoloration and lipid oxidation in muscle and meat, *Quim. Nova*, 2006, **29**, 1270.

38 C. A. Rice-Evans, Formation of free radicals and mechanisms of action in normal biochemical processes and pathological states, *New Compr. Biochem.*, 1994, **28**, 131.

39 M. R. Richards, Redox Reactions of Myoglobin, *Antioxid. Redox Signaling*, 2010, **18**, 2342.

40 U. Flögel, A. Gödecke, L.-O. Klotz and J. Schrader, Role of myoglobin in the antioxidant defense of the heart, *FASEB J.*, 2004, **18**, 1156.

41 M. P. Richards, J. G. Whalin, Y. Wu, S. P. Suman, Y. Wang and J. L. Shohet, Myoglobin and Hemoglobin: Discoloration, Lipid Oxidation, and Solvent Access to the Heme Pocket, *Meat Muscle Biol.*, 2023, **6**, 14400.

42 L.-S. Fan and K. Tsuchiya, *Bubble wake dynamics in liquids and liquid-solid suspensions*, Butterworth-Heinemann, 1990.

43 S. S. Sadhal, P. S. Ayyaswamy and J. N. Chung, Formation and Breakup of Bubbles and Drops, *Transport Phenomena with Drops and Bubbles, Mechanical Engineering Series*, Springer, New York, NY, 1997, DOI: [10.1007/978-1-4612-4022-8\\_7](https://doi.org/10.1007/978-1-4612-4022-8_7).

44 J. Zahradník and M. Fialová, The effect of bubbling regime on gas and liquid phase mixing in bubble column reactors, *Chem. Eng. Sci.*, 1996, **51**, 2491.

45 N. K. Kyriakides, E. G. Kastrinakis, S. G. Nychas and A. Goulas, Bubbling from nozzles submerged in water: transitions between bubbling regimes, *Can. J. Chem. Eng.*, 1997, **75**, 684.

46 J. M. Chawla, 1985, Atomisation of Liquids Employing the Low Sonic Velocity in Liquid/Gas Mixtures, Proceedings of the 3rd International Conference on Liquid Atomization and Spray Systems, London, United Kingdom, pp. LP/1A/5/1-7.

47 D. J. McCann and R. G. Prince, “Regimes of Bubbling at a Submerged Orifice”, *Chem. Eng. Sci.*, 1971, **26**, 1505–1512.

48 I. Miyahara, N. Haga and T. Takahashi, “Bubble Formation from an Orifice”, *Int. Chem. Eng.*, 1983, **23**, 524–531.

49 I. Leibson, E. Holcomb, A. Cacoso and J. Jasmic, Rate of Flow and Mechanics of Bubble Formation from Single Submerged Orifices, *AIChE J.*, 1956, **2**, 296.

50 C. Mulbah, C. Kang, N. Mao, W. Zhang, A. Raza Shaikh and S. Teng, A review of VOF methods for simulating bubble dynamics, *Prog. Nucl. Energy*, 2022, **154**, 104478.

51 A. Man Zhang, S.-M. Li, P. Cui and S. Li, Unified theory for bubble dynamics, *Phys. Fluid*, 2023, **35**, 033323.

52 J. Pablo Trelles, Advances and challenges in computational fluid dynamics of atmospheric pressure plasmas, *Plasma Sources Sci. Technol.*, 2018, **27**, 093001.

53 H. B. Al Babaa, T. Elgammal and R. S. Amano, Correlations of Bubble Diameter and Frequency for Air-Water System Based on Orifice Diameter and Flow Rate, *J. Fluids Eng.*, 2016, **138**, 11, DOI: [10.1115/1.4033749](https://doi.org/10.1115/1.4033749).

54 W. Siemes and J. F. Kaufmann, *Chem. Eng. Sci.*, 1956, **5**, 127.

55 Y.-F. Zhao and G. A. Irons, The breakup of bubbles into jets during submerged gas injection, *Metall. Trans. B*, 1990, **21**(6), 997–1003, DOI: [10.1007/BF02670270](https://doi.org/10.1007/BF02670270).

56 J. San Lee, B. Mook Weon, S. Ji Park, J. Ho Je, K. Fezzaa and W.-K. Lee, Size limits the formation of liquid jets during bubble bursting, *Nat. Commun.*, 2011, **2**, 367.

57 D. Jourd'heuil, L. Mills, A. M. Miles and M. B. Grisham, Effect of nitric oxide on hemoprotein-catalyzed oxidative reactions, *Nitric oxide*, 1998, **2**(1), 37–44.

58 H. M. Nguyen, B. Nair, T. T. Nguyen, J. Leon Shohet and H. D. Le, Detection and optimization of 2-hydroxyterephthalic acid formed through the reaction of terephthalic acid with hydroxyl radical in liquid exposed to helium cold atmospheric plasma jet, *Plasma Sci. Technol.*, 2025, **17**, 125504, DOI: [10.1088/2058-6272/ae0c78](https://doi.org/10.1088/2058-6272/ae0c78).

59 N. Yawu, T. Mekwilai, N. Vichiansan, S. Braspaiboon, K. Leksakul and D. Boonyawan, Cold plasma technology: Transforming food processing for safety and sustainability, *J. Agric. Food Res.*, 2024, **18**, 101383.

60 R. Sharma, P. Chandra Nath, S. Rustagi, M. Sharma, B. Stephen Inbaraj, P. Kumar Dikkala, P. Kumar Nayak and K. Sridhar, Cold Plasma—A Sustainable Energy-Efficient Low-Carbon Food Processing Technology: Physico-chemical Characteristics, Microbial Inactivation, and Industrial Applications, *Int. J. Food Sci.*, 2025, 4166141.

61 A. Komuro, Review of streamer discharge-induced plasma chemistry at atmospheric pressure: Key mechanisms and future perspectives, *J. Electrost.*, 2025, **137**, 104087.



62 L. Miles, B. Nair, H. M. Nguyen, T. Aiken, J. L. Shohet and H. D. Le, Cold Atmospheric Plasma Selectively Targets Neuroblastoma: Mechanistic Insights and In Vivo Validation, *Cancers*, 2025, **17**(21), 3432, DOI: [10.3390/cancers17213432](https://doi.org/10.3390/cancers17213432).

63 N. N. Misra, V. P. Sreelakshmi, T. Naladala, K. J. Alzahrani and P. S. Negi, Design and construction of a continuous industrial scale cold plasma equipment for fresh produce industry, *Innovative Food Sci. Emerging Technol.*, 2024, **97**, 103840.

